International Journal of Automation and Computing 8(3), August 2011, 348-356
DOI: 10.1007/s11633-011-0591-3

Self-contained Capsubot Propulsion Mechanism

M. Nazmul Huda Hong-Nian Yu Samuel Oliver Wane
Faculty of Computing, Engineering and Technology, Staffordshire University, Stafford ST18 0AD, UK

Abstract: In this paper, a self contained capsubot (capsule robot) propulsion mechanism is investigated. The proposed capsubot works on the principle of internal force-static friction. A modified linear DC motor is used to drive the capsubot. A novel acceleration profile is proposed for the moving part (linear cylinder) based on the principle. A significant feature of the proposed capsubot is that it is legless, wheelless, and trackless. The developed capsubot with a proposed propulsion mechanism demonstrates a very good average velocity. The propulsion mechanism has the potential to be used for the propulsion of a wireless-controlled self-propelling capsule endoscope. Simulation and experimental results demonstrate the performance of the self-contained capsubot with the proposed acceleration profile.

Keywords: Capsubot, internal force and static friction, linear DC motor, propulsion, capsule endoscopy.

1 Introduction

In 1950, the invention of the gastro-camera opened a new era in medical science which made it possible to investigate the oesophagus, the stomach, the upper small bowel and colon. Initially, a push pipe was used to carry the camera, but the invention of optical fibre in 1960 replaced the push pipe and made the investigation less invasive[1]. In 2000, Given Imaging introduced a wireless video capsule for the investigation of the small bowel which is virtually a non-invasive process[2]. Later on, capsule endoscopes were developed for the oesophagus and colon with modified designs[3]. Though capsule endoscopy has many advantages over traditional wired endoscopy, it has no control over its motion. The capsule goes from mouth to anus with the aid of peristalsis and gravity. The capsule cannot go back to scan a suspected region and also cannot stop or distend tissue for better observation. Moreover, there is still no capsule endoscope that can be used to inspect the stomach due to its large diameter. A wireless-controlled and self-propelling capsule endoscope can be a solution to these issues. Researchers have assessed suitable propulsion techniques for capsubot locomotion. Some are designed by mimicking insects: earth-worm[4], inch-worm[5] or a human paddling a canoe[6]; others used the internal force-static friction principle[7] or a magnetic field[8].

For propulsion, several mechanisms can be used e.g., 1) external propulsion (wheeled[9, 10], legged[11], tracked[12, 13], and wheeled-legged[14]), 2) internal propulsion[7], and 3) hybrid propulsion[15]. All four external propulsions have been used in developing robots for rescue purposes[14, 16]. A wheeled robot has been developed to assist the surgeon during laparoscopic surgery in the abdominal cavity[9]. However, to develop robots for wireless-capsule-endoscopy (WCE), only legged propulsion is used among the four external propulsions. Many legged designs, e.g., 3-legged[17, 18], 4-legged[19], 12-legged[11], paddling based[6], earthworm-like[4], and inchworm-like[5] propulsion principles have been proposed by researchers. Legged locomotion has some advantages: it can pass through narrow places by distending the tissue by legs; it can use its legs to distend tissue for better observation and, if adhesive is attached to the legs, it can resist dislodgement while moving. However, at the same time, legged locomotion has some constraints, which prevent it being an ideal choice for the capsubot design. The complex structure and high battery requirement make it difficult to build a capsule with this mechanism sufficiently small. Moreover, the sharp edges of the legs create high risk of injury to the patient.

For internal propulsion, there are no legs, wheels or limbs outside the body. Some internal propulsion based designs, e.g., internal force-static friction based[7], magnetic field based[20, 21], magnetic resonance imaging (MRI) based[22] capsubot designs are also proposed. In the case of internal force-static friction, a permanent magnet is placed in a peripheral coil wound cylindrical body. By controlling the energizing of the coil, the cylindrical body can be moved linearly. An open loop control strategy is adopted in [7]. A closed loop control approach is developed in [23] for a pendulum-driven cart-pole system that can be used to demonstrate the dynamics and control challenges faced in a capsule robot. A seven-step optimization and a closed loop simple-switch control strategy are proposed in [24]. In the case of a controlled magnetic field, the capsubot can move linearly and rotationally. An external magnetic field is applied to the magnetic shell coated video capsule[21]. However, magnetic material near the patient can distract the motion of the capsule. Another option is to use ferromagnetic material instead of a magnet in the capsule[22]. However, in that case a very high external magnetic field is necessary, which increases the cost. In [8], static and radio frequency (RF) magnetic fields of MRI are used for propulsion. A static magnetic field is used for producing propulsion force and an RF magnetic field is used to provide power. Hybrid locomotion is the combination of internal legged actuation mechanisms and external magnetic dragging[15].

This paper investigates the legless motion of a capsule robot studied in [7, 23, 24] in the principle of internal

Manuscript received November 15, 2010; revised January 12, 2011
This work was supported by EPSRC funded UK-Japan Network on Human Adaptive Mechatronics Project (No. EP/E025250/1) and EU Erasmus Mundus Project-eLINK (No. EM ECW-ref.149674-EM-1-2008-1-UK-ERAMUNDUS)

force-static friction. In this research, a prototype of the legless capsubot propulsion system based on the above mentioned principle, has been implemented in a self-contained format. The inner mass (cylinder of a linear motor) of the capsubot follows a new four-step acceleration profile. A control law is developed for the motion control of the capsubot. The implemented capsubot is stable and moves forward with a smooth and satisfactory average velocity.

The paper is structured as below. Section 2 investigates the modeling of the capsubot. Motion generation is considered in Section 3. Section 4 concentrates on the control of the capsubot. The simulation results with analysis are shown in Section 5. Section 6 describes the hardware of the capsubot system. Section 7 describes the experiments and shows experimental results. In Section 8, analysis and validation is presented. Finally, Section 9 is dedicated for conclusions and future work.

2 Modelling of the capsubot

The basic structure of the capsubot is shown in Fig. 1. By moving the inner mass (moving part) back and forth with controlled acceleration, the capsubot can be moved in a certain given direction.

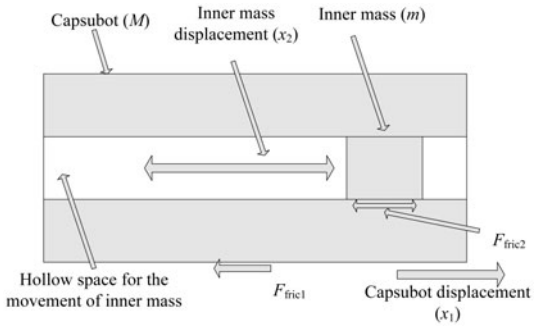

Fig. 1 Schematic diagram of the capsubot

According to Newton′s laws, the motion equations for the cylinder and the capsubot are:

$$F = ma_2 + F_{\text{fric2}} \tag{1}$$

$$F_r = -ma_2 = Ma_1 + F_{\text{fric1}} \tag{2}$$

where F is linear force applied on the inner mass (m), which makes it move with a_2 acceleration, F_r is the reaction force that may move the capsubot (M) in the opposite direction of the force with a_1 acceleration, $F_{\text{fric2}} = \text{sgn}(\dot{x}_2 - \dot{x}_1)\mu_2 Mg$ is the friction force between the cylinder and the capsubot; $F_{\text{fric1}} = \text{sgn}(\dot{x}_1)\mu_1 Mg$ is the friction force between the capsubot and the surface of motion.

Using (1) in (2), we have

$$-F = Ma_1 + F_{\text{fric1}} - F_{\text{fric2}}. \tag{3}$$

Thus, (1) and (3) are the motion equations for the inner mass and the capsubot, respectively.

3 Motion generation analysis

The implemented capsubot is shown in Fig. 2. Here, the cylinder of the linear motor works as an inner mass. When the cylinder accelerates in a certain direction, the capsubot receives a force in the opposite direction. This force results in moving the capsubot in a certain direction. The cylinder follows the 4-step acceleration profile shown in Fig. 3. The motions of the cylinder and the capsubot system are shown in Fig. 4.

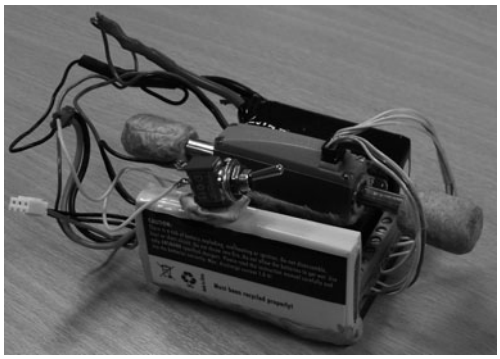

Fig. 2 Self-contained capsubot system

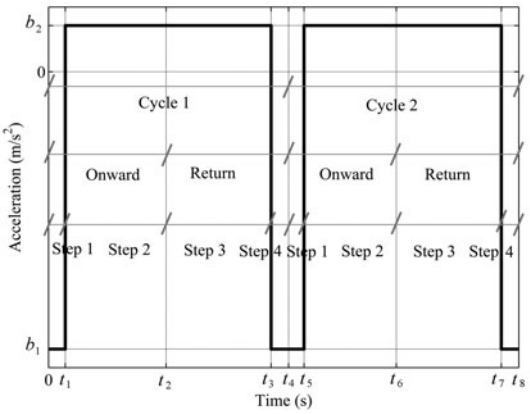

Fig. 3 Proposed acceleration profile

3.1 The four-step motion of the capsubot

Initialization. The cylinder is placed in the center position of the motor housing and the motion controller is switched on. The cylinder starts moving forward and travels half of the stroke length, i.e., 9 mm, and stops. Now, the capsubot is ready to start cycle 1. Initialization is needed only before cycle 1. As the friction force dominates over the reaction force, the capsubot remains standstill during initialization.

Cycle 1 (Initial cycle):

Step 1. The cylinder moves backward with a high $-ve$ accelerated motion and the capsubot receives a force in the forward direction. Here, the reaction force is big enough to overcome the friction. Thus, the capsubot moves forward with a $+ve$ accelerated motion.

Step 2. It comprises of 2 sub-steps: 2 (i) and 2 (ii). The cylinder continues to move backward but with a small $+ve$ accelerated motion for the whole Step 2. The capsubot moves forward with a small $-ve$ accelerated motion in 2 (i) before it stops. The capsubot remains standstill in Step 2 (ii) as the friction force dominates over the reaction force. The cylinder reaches its left limit of movement (-9 mm position) at the end of Step 2 and stops. It instantaneously reverses its direction of movement and Step 3 begins.

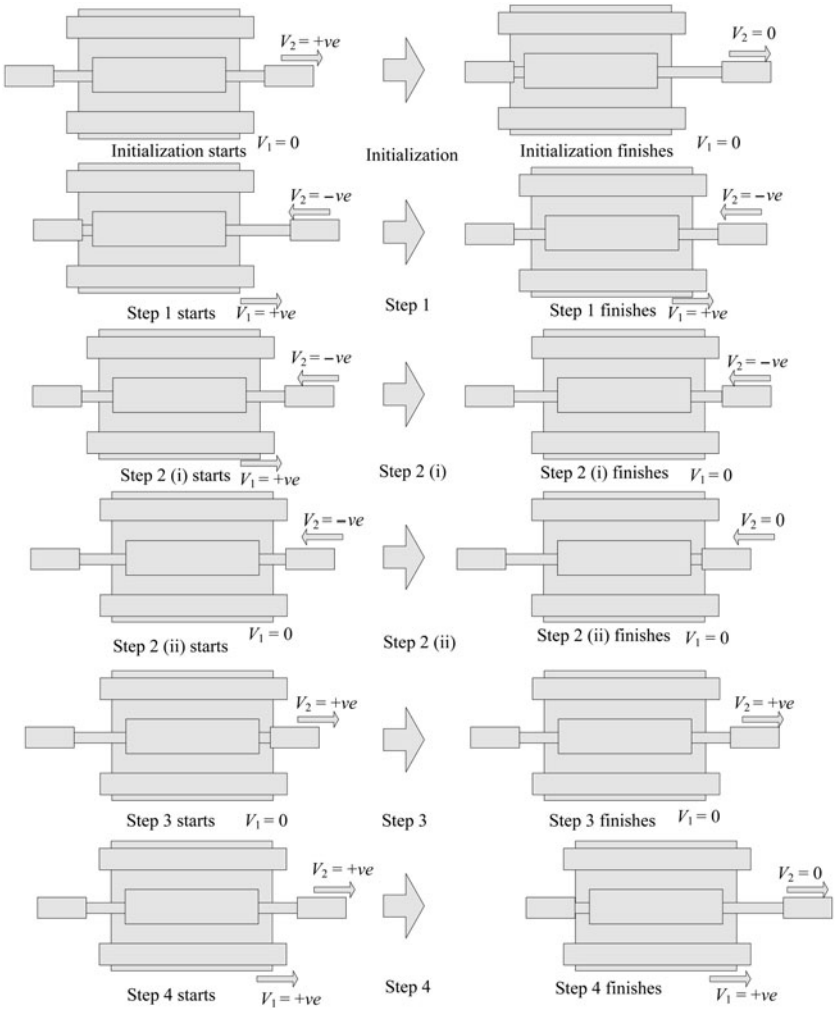

Fig. 4 Four-step motion of the capsubot (4 steps complete one cycle)

Step 3. The cylinder moves forward slowly with a small $+ve$ acceleration and, as the friction force dominates, the capsubot remains standstill.

Step 4. The cylinder moves forward with a high $-ve$ accelerated motion and the capsubot moves forward with a $+ve$ acceleration. The cylinder reaches its right limit of movement (9 mm position) at the end of this step and stops. It instantaneously reverses its direction and Step 1 of cycle 2 begins.

Cycle 2 (Repeated cycle):

Step 1. Unlike Step 1 of cycle 1, here the capsubot has a $+ve$ initial velocity. Thus, the capsubot travels a longer distance in this step than it travels in Step 1 of cycle 1. It continues to move for the next step.

Step 2. Same as Step 2 of cycle 1 but here the caspubot keeps moving for a longer time than in cycle 1 and thus the travelled distance is also greater.

Step 3. Same as Step 3 of cycle 1.

Step 4. Same as Step 4 of cycle 1.

Remaining cycles are same as cycle 2.

By repeating the cycles, the capsubot is moved forward. The capsubot moves in Steps 4 and 1, and a portion of Step 2 and it remains stationary for the remaining time. By changing the acceleration direction of the cylinder, the capsubot can be moved in the opposite direction. By changing the acceleration magnitude, the capsubot can be moved with different average velocities.

4 Control law of the capsubot

The desired inner mass acceleration, $\ddot{x}_{2d}$ is taken from the optimal acceleration profile:

$$\ddot{x}_{2d} = \begin{cases} b_1, & t \in [0, t_1) \\ b_2, & t \in [t_1, t_3) \\ b_1, & t \in [t_3, t_5) \\ b_2, & t \in [t_5, t_7) \\ b_1, & t \in [t_7, t_8]. \end{cases}$$

By integrating the above equation, the desired inner mass velocity, $\dot{x}_{2d}$, can be defined as

$$\dot{x}_{2d} = \begin{cases} b_1 t + \dot{x}_{2d}(0), & t \in [0, t_1) \\ b_2(t - t_1) + \dot{x}_{2d}(t_1), & t \in [t_1, t_3) \\ b_1(t - t_3) + \dot{x}_{2d}(t_3), & t \in [t_3, t_5) \\ b_2(t - t_5) + \dot{x}_{2d}(t_5), & t \in [t_5, t_7) \\ b_4(t - t_7) + \dot{x}_{2d}(t_7), & t \in [t_7, t_8]. \end{cases}$$

From (2), the motion equation of the capsubot is

$$\begin{aligned} -m_2\ddot{x}_2 &= M\ddot{x}_1 + \mathrm{sgn}(\dot{x}_1)\mu_1 Mg \\ \text{or} \quad \ddot{x}_1 &= \frac{1}{M}(-m_2\ddot{x}_2 - \mathrm{sgn}(\dot{x}_1)\mu_1 Mg)t \end{aligned} \tag{4}$$

where

$$\mathrm{sgn}(\dot{x}) = \begin{cases} 1, & \text{if } \dot{x} > 0 \\ 0, & \text{if } \dot{x} = 0 \\ -1, & \text{if } \dot{x} < 0. \end{cases}$$

The capsubot remains standstill in a portion of Step 2 and in Step 3 and, keeps moving forward for the remaining time. Thus, by integrating (4), the desired velocity of the capsubot $\dot{x}_{1d}$ can be defined as

$$\dot{x}_{1d} = \begin{cases} \frac{1}{M}(-m_2 b_1 - \mu_1 Mg)t + \dot{x}_{1d}(0), & t \in [0, t_1) \\ \frac{1}{M}(-m_2 b_2 - \mu_1 Mg)(t - t_1) + \dot{x}_{1d}(t_1), & t \in [t_1, t_{s1}) \\ 0, & t \in [t_{s1}, t_3) \\ \frac{1}{M}(-m_2 b_1 - \mu_1 Mg))(t - t_3), & t \in [t_3, t_5) \\ \frac{1}{M}(-m_2 b_2 - \mu_1 Mg)t + \dot{x}_{1d}(t_5), & t \in [t_5, t_{s2}) \\ 0, & t \in [t_{s2}, t_7) \\ \frac{1}{M}(-m_2 b_1 - \mu_1 Mg)(t - t_7), & t \in [t_7, t_8]. \end{cases}$$

The values of b_1 to b_4, t_1 to t_8, t_{s1}, and t_{s2}, are optimally selected considering the system constraints. The details of optimal selection of the parameters can be found in [25].

Open loop control law. Using the equations of $\ddot{x}_{2d}$, $\dot{x}_{2d}$, and $\dot{x}_{1d}$ in (1), the open loop control law can be defined as

$$F_d = m\ddot{x}_{2d} + \mathrm{sgn}(\dot{x}_{2d} - \dot{x}_{1d})\mu_2 mg. \tag{5}$$

All the simulations in this paper are performed using Matlab and Simulink with the help of the control law of (5) and motion equations (1) and (3).

5 Simulation results

The parameters of the implemented capsubot are presented in Table 1. The optimum parameters of the proposed acceleration profile are presented in Table 2 using the equations from [25]. The simulation results are shown in Figs. 5–10. During simulation the friction coefficient of the capsubot with a plywood table was used.

Table 1 Parameters of the capsubot

Parameters	Explanations	Values
M	Total mass of the capsubot	0.3216 kg
m_2	Mass of the cylinder with extra mass	0.050 kg
μ_1	Dynamic friction coefficient between capsubot and surface of movement (plywood table)	0.08
μ_2	Dynamic friction coefficient between the capsule shell and the cylinder	0.2
g	Acceleration of gravity	9.8 m/s^2
	Total stroke length in one direction	0.018 m

Table 2 Optimum parameters of acceleration profile for the developed capsubot

Parameters	Values	Parameters	Values
t_1	0.013	t_{s2}	0.254
t_{s1}	0.044	t_6	0.263
t_2	0.089	t_7	0.342
t_3	0.168	t_8	0.342
t_4	0.181	b_1	−30 m/s^2
t_5	0.193	b_2	5 m/s^2

In Fig. 5, the maximum control force used is 1.6 N. In Steps 1 and 4, the control force creates same accelerations yet control force is higher for Step 1 than in Step 4. This is because in Step 1, the control force needs to create a $-ve$ acceleration and overcome the frictional force, whereas in Step 4 frictional force is added to the control force to create a $-ve$ acceleration. Similarly, in Step 2, frictional force is added to the control force to create a $+ve$ acceleration whereas in Step 3 control force creates $+ve$ acceleration and overcomes the frictional force. Thus, control force is higher in Step 3 than in Step 2. The same force profile is repeated in every cycle.

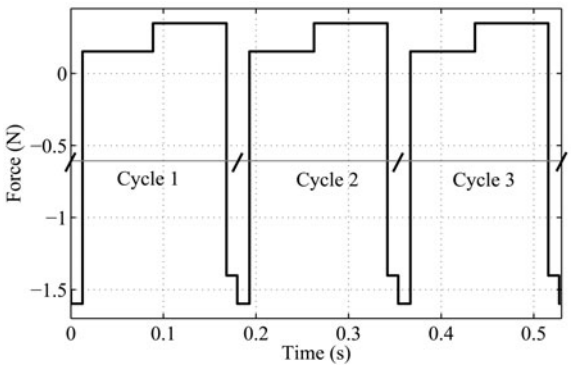

Fig. 5 Control force on the cylinder for three cycles

Fig. 6 shows simulated accelerations of the cylinder and the capsubot. Steps 1 and 4 provide a high $-ve$ acceleration whereas Steps 2 and 3 provide a low $-ve$ acceleration for the cylinder. The capsubot remains standstill in Step 3. The capsubot has a $+ve$ acceleration in Step 1 and has a $-ve$ acceleration in a portion of Step 2 and finally it stops. The capsubot maintains a zero acceleration in the rest of Steps 2 and 3. In Step 4, the capsubot has a $+ve$ acceleration,

which continues in Step 1 of cycle 2. In Step 2 of cycle 2, the capsubot maintains a $-ve$ acceleration for a longer time than in cycle 1, as the capsubot reaches a higher velocity at the end of Step 1 of cycle 2 than in cycle 1. Beginning from the second cycle, the acceleration pattern of the capsubot for all the cycles are the same.

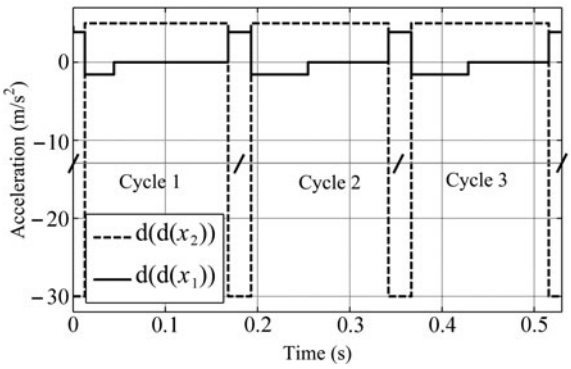

Fig. 6 Simulated accelerations for three cycles

In Fig. 7, simulated velocities for the cylinder and the capsubot are shown. The cylinder performs a higher rate of changes of velocity in Steps 1 and 4, and performs a lower rate of changes of velocity in Steps 2 and 3. The velocity of the capsubot increases in Step 1 and decreases in Step 2 and reaches zero in the middle of Step 2. It remains zero for the rest of Steps 2 and 3. Again the velocity of the capsubot starts increasing in Step 4 and it continues to increase in Step 1 of the next cycle and then decreases in Step 2 and reaches zero during Step 2. Beginning from cycle 2, the velocity of the capsubot reaches a higher value at the end of Step 1 than in cycle 1, because from cycle 2 the capsubot has a nonzero initial velocity at the beginning of Step 1.

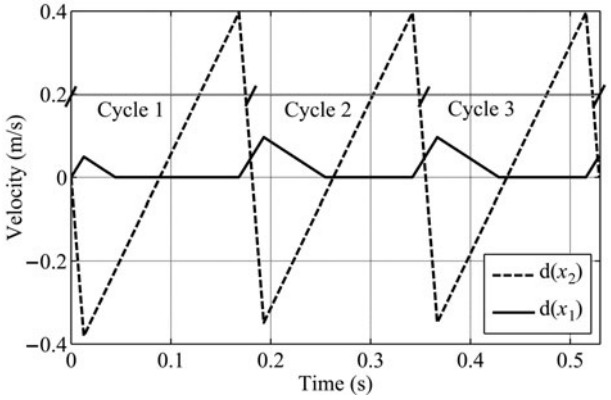

Fig. 7 Simulated velocities for three cycles

Fig. 8 shows the absolute position of the cylinder, absolute position of the capsubot and relative position of the cylinder with respect to the mid-point of the housing of the linear motor. The relative position of the cylinder is confined within ±9 mm which proves the stability of the system.

Fig. 9 shows the effect of the cylinder acceleration on the position of the capsubot. The capsubot moves forward in Step 1, a portion of Steps 2 and 4, and remains stationary for the remaining time. The capsubot starts moving forward when the cylinder starts moving with a high $-ve$ acceleration. The travelled distance in cycle 2 and forthcoming cycles is higher than that of cycle 1, because from cycle 2 the capsubot has a $+ve$ initial velocity as the capsubot starts moving forward from Step 4 of the previous cycle. It is the special feature of the proposed acceleration profile.

Fig. 10 shows the phase plane plot of the cylinder. It shows that the cylinder follows a high acceleration when it is within the position 6 mm to 9 mm and it follows a small acceleration when it is within the position of −9 mm to 6 mm.

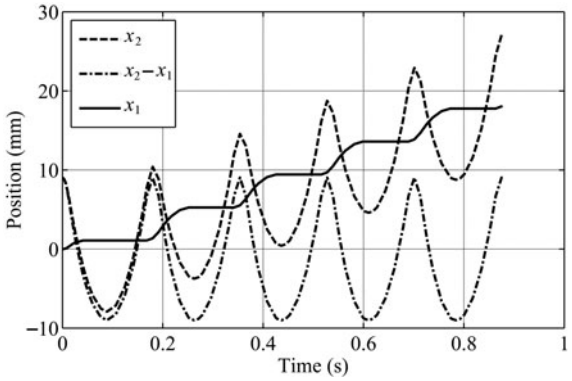

Fig. 8 Simulated positions for five cycles

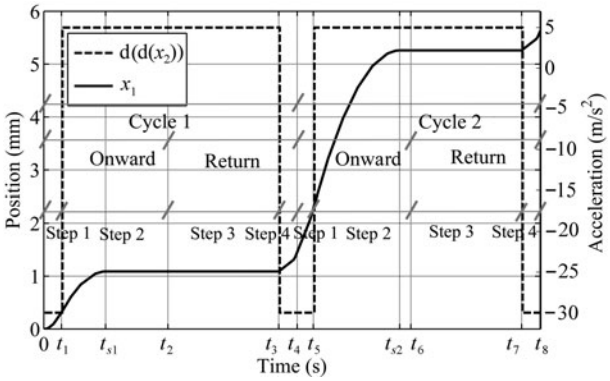

Fig. 9 Simulated position of the capsubot with the acceleration of the cylinder

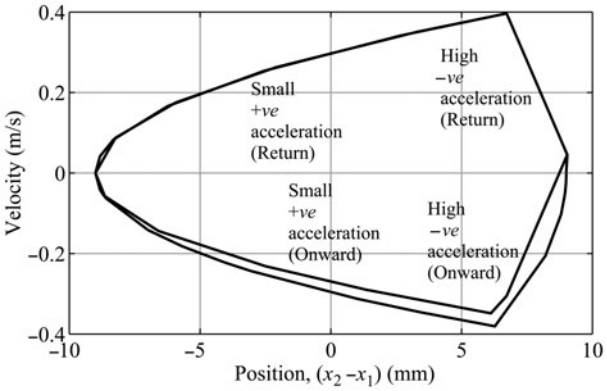

Fig. 10 Simulated phase plane plot of the cylinder

6 Hardware of the capsubot system

A practical experiment has been conducted and described in this paper. Here, a linear DC motor (QUICKSHAFT

LM1247-020-01)[26] is used to drive the capsubot system. The propulsion mechanism based on the internal force-static friction is utilized. The linear motor is modified to serve our purpose. The modified linear motor is shown in Fig. 11. It comprises of a housing or motor shell, which houses the coil and a cylindrical rod, which is a permanent magnet.

Fig. 11 Modified linear DC motor

The complete capsubot system is shown in Fig. 2 and the dimensions are shown in Fig. 12. The main components of the capsubot are a linear motor, a motion controller and two batteries. The motion of the cylinder is controlled by the motion controller. A linear force is applied to the cylinder when the coil in the motor housing is energized by the motion controller. The maximum force that can be applied is 9.26 N, whereas the continuous force is 3.09 N. At both ends of the cylinder 16 grams of mass has been added to result in greater displacement of the capsubot.

Two Lipo Lithium-ion batteries[27] of 7.4 V are used to power the linear DC motor. There are Hall sensors in the housing of the DC motor by which the position of the cylinder is tracked and fed back to the motion controller to form a closed loop system.

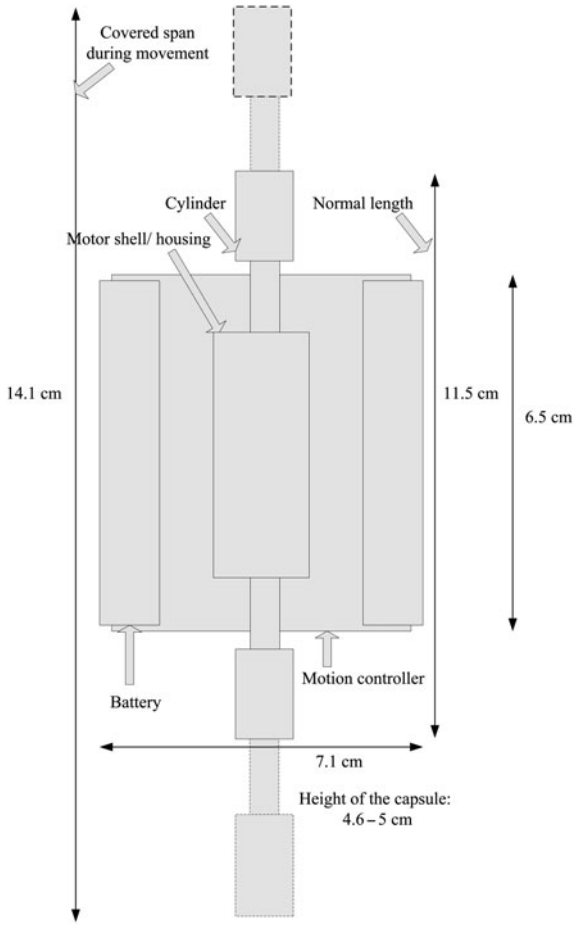

Fig. 12 Dimensions of the capsubot system

7 Experiments

The motion controller of the capsubot system is programmed using the Motion Manager Software[26] and the program is transferred from PC to the motion controller by an RS-232 cable and stored in the EEPROM of the motion controller. The motion controller is disconnected from the PC and the self contained capsubot propulsion system is formed by putting all the elements in place. Whenever the motion controller is powered, the program is downloaded from the EEPROM to the working memory of the motion controller and it executes the program. The controller is programmed to move the cylinder from one location to another by using an input acceleration and deceleration. The controller by itself calculates the time it has to use for acceleration and then deceleration to reach the desired location. The controller uses three hall sensors that are placed on the housing of the motor to take feedback about the position of the cylinder and corrects the input to the cylinder accordingly to maintain the desired acceleration or deceleration and velocity.

The experimental results are shown in Figs. 13–16. The data are obtained from the Motion Manager Software and then the curves are plotted using Matlab. The experiment was done on different surfaces and we found that the cylinder movement is consistent and independent of the surface friction. The average velocity of the capsubot was measured between 0.76 cm/s (on carpet) to 2 cm/s (on a plywood table).

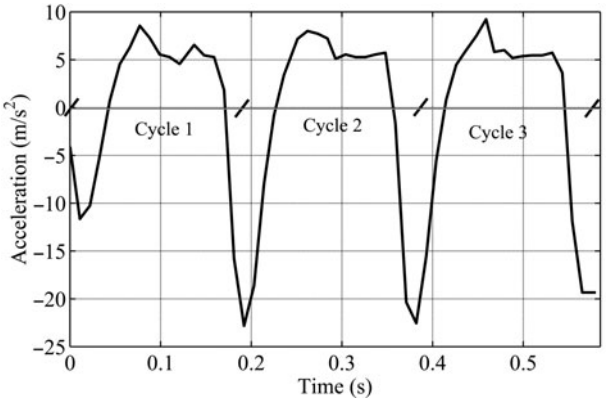

Fig. 13 Experimental acceleration of the cylinder for three cycles

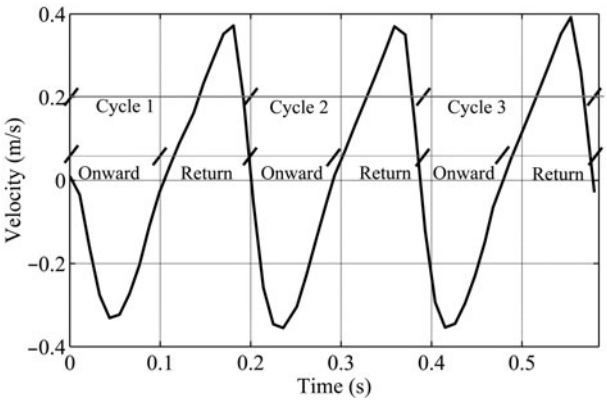

Fig. 14 Experimental velocity of the cylinder for three cycles

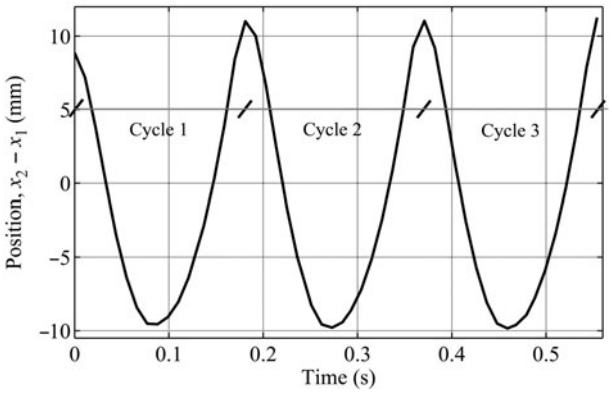

Fig. 15 Experimental position of the cylinder for three cycles

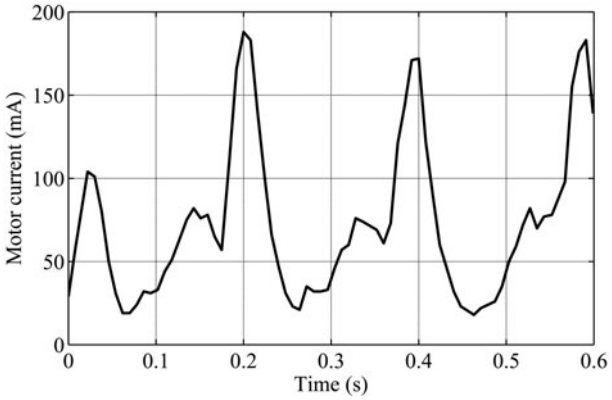

Fig. 16 Experimental motor current for three cycles

Fig. 13 shows the experimental acceleration of the cylinder. It shows that experimentally the capsubot cannot perform a sharp transition between the accelerations. The motion controller corrects the acceleration to make the movement of the cylinder according to the programmed one. In the second step, the cylinder experiences a higher deceleration than expected to stop the cylinder at the end of its onward journey.

Fig. 14 shows the experimental velocity of the cylinder. Here, the cylinder follows a higher rate of changes of velocity in Steps 1 and 4, and a lower rate of changes of velocity in Steps 2 and 4 as expected.

Fig. 15 shows the experimental position of the cylinder with respect to the mid-point of the linear motor housing.

Fig. 16 shows the experimental current consumption of the capsubot. The current consumption increases with the increase of the absolute value of the acceleration. The average current that the linear motor consumes is calculated as 0.0732 A. Supply from the battery was 14.8 V DC. The average power requirement of the capsubot is 1.08 W. One of the batteries is 1000 mA·h and the other is 800 mA·h. Thus, the capsubot can be operated for 10 h and 55 min before the batteries need to be charged again.

8 Analysis and validation

Figs. 17–20 compare the experimental results with the simulation results.

Fig. 17 compares the acceleration of the cylinder. The experimental operation spends more time than that of the simulated operation. The acceleration changes slowly in the experimentation; it did not allow the sharp transition like the simulation.

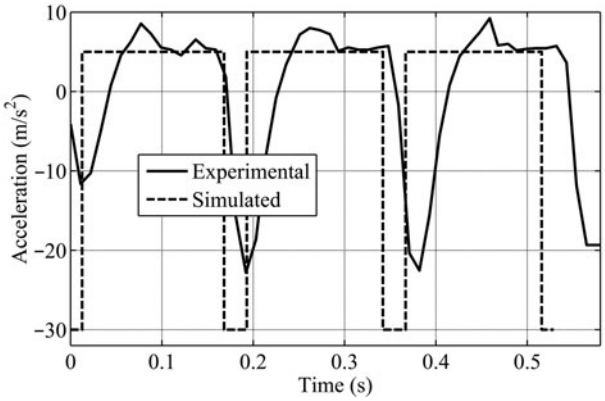

Fig. 17 Acceleration of the cylinder for three cycles

Fig. 18 compares the velocity of the cylinder. Here, the experimental operation spends more time in every step compared to the simulated operation. Otherwise, the pattern of both experimentation and simulation are quite similar.

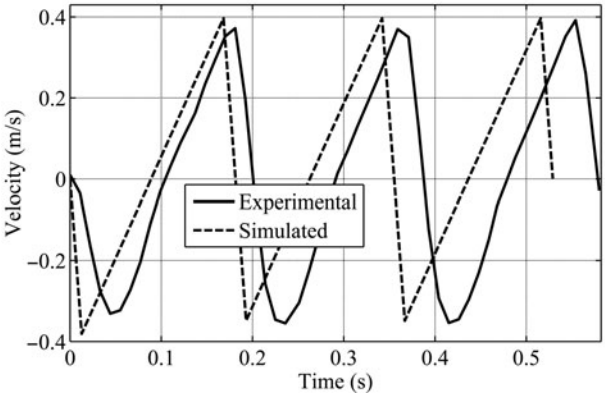

Fig. 18 Velocity of the cylinder for three cycles

Fig. 19 compares the relative position of the cylinder. The experimental result matches with the simulated result in the first cycle and then from the second cycle experimental result took slightly more time than the simulated one. However, the shape of the curve at each cycle is almost similar for both results except the peaks.

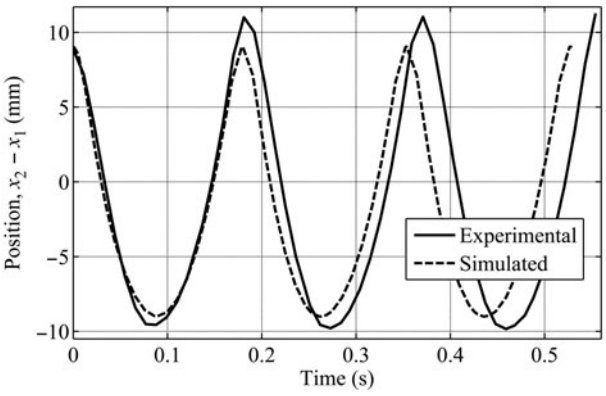

Fig. 19 Position of the cylinder for three cycles with respect to the mid-point of the capsubot

Fig. 20 is drawn from the experimental and simulated data for the movement of the capsubot on a plywood table. The experimental velocity is less than the simulated one. The difference between the two results is smaller for a higher acceleration.

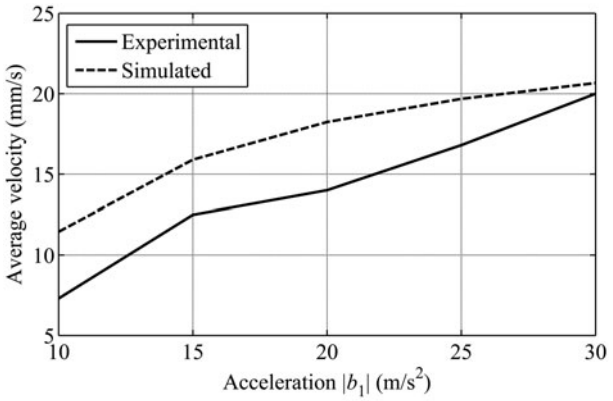

Fig. 20 Average velocity of the capsubot for different first and fourth steps acceleration

The small difference that we observe between the simulated and the experimental results may arise from the simple model that we have used in the motion equation. We have neglected the motor dynamics, the viscous, and Stribeck frictions[28] and, other disturbances in our simulation model. A more practical model incorporating a more robust friction model and other parameters would improve the simulation results.

9 Conclusions

The simulation and experimental results show the performance of the proposed acceleration profile. The uniqueness of the proposed acceleration profile is that the capsubot moves forward even when the cylinder is returning to its initial position. Previous papers[7, 23, 24] written on this principle do not show this performance. The implemented capsule is self contained and more importantly legless yet demonstrates a high average velocity. This propulsion mechanism can be integrated with the currently available capsule endoscopes and thus can decrease the total time of inspection. By varying the acceleration of the cylinder in Steps 1 and 4, the average velocity of the capsubot can be varied. Thus, the capsubot can move fast or slow or can stop for sometime according to the requirements.

References

[1] Y. Kusuda. A further step beyond wireless capsule endoscopy. *Sensor Review*, vol. 25, no. 4, pp. 259–260, 2005.

[2] G. Iddan, G. Meron, A. Glukhovsky, P. Swain. Wireless capsule endoscopy. *Nature*, vol. 405, no. 6785, pp. 417, 2000.

[3] A. Moglia, A. Menciassi, P. Dario, A. Cuschieri. Capsule endoscopy: Progress update and challenges ahead. *Nature Reviews Gastroenterology and Hepatology*, vol. 6, no. 6, pp. 353–361, 2009.

[4] S. Park, J. Park, H. Park, S. Park, C. Jee, S. Park, B. Kim. Multi-functional capsule endoscope for gastrointestinal tract. In *Proceedings of SICE-ICASE International Joint Conference*, IEEE, Busan, Korea, pp. 2090–2093, 2006.

[5] B. Kim, S. Park, J. Park. Microrobots for a capsule endoscope. In *Proceedings of IEEE/ASME International Conference on Advanced Intelligent Mechatronics*, IEEE, pp. 729–734, 2009.

[6] H. Park, S. Park, E. Yoon, B. Kim, J. Park, S. Park. Paddling based microrobot for capsule endoscopes. In *Proceedings of IEEE International Conference on Robotics and Automation*, IEEE, pp. 3377–3382, 2007.

[7] H. Y. Li, K. Furuta, F. L. Chernousko. Motion generation of the capsubot using internal force and static friction. In *Proceedings of the 45th IEEE Conference on Decision and Control*, IEEE, pp. 6575–6580, 2006.

[8] G. Kosa, P. Jakab, F. Jolesz, N. Hata. Swimming capsule endoscope using static and RF magnetic field of MRI for propulsion. In *Proceedings of IEEE International Conference on Robotics and Automation*, IEEE, pp. 2922–2927, 2008.

[9] M. E. Rentschler, J. Dumpert, S. R. Platt, K. Lagnernma, D. Oleynikov, S. M. Farritor. Modeling, analysis, and experimental study of in vivo wheeled robotic mobility. *IEEE Transactions on Robotics*, vol. 22, no. 2, pp. 308–321, 2006.

[10] Y. Liu, M. Hasan, H. Yu. Modelling and remote control of an excavator. *International Journal of Automation and Computing*, vol. 7, no. 3, pp. 349–358, 2010.

[11] S. Gorini, M. Quirini, A. Menciassi, G. Pernorio, C. Stefanini, P. Dario. A novel SMA-based actuator for a legged endoscopic capsule. In *Proceedings of the 1st IEEE/RAS-EMBS International Conference on Biomedical Robotics and Biomechatronics*, IEEE, Pisa, Italy, pp. 443–449, 2006.

[12] J. Suthakorn, S. Shah, S. Jantarajit, W. Onprasert, W. Saensupo, S. Saeung, S. Nakdhamabhorn, V. Sa-Ing, S. Reaungamornrat. On the design and development of a rough terrain robot for rescue missions. In *Proceedings of IEEE International Conference on Robotics and Biomimetics*, IEEE, Bangkok, Thailand, pp. 1830–1835, 2009.

[13] Y. H. Zweiri. Identification schemes for unmanned excavator arm parameters. *International Journal of Automation and Computing*, vol. 5, no. 2, pp. 185–192, 2008.

[14] M. Eich, F. Grimminger, F. Kirchner. Proprioceptive control of a hybrid legged-wheeled robot. In *Proceedings of IEEE International Conference on Robotics and Biomimetics*, IEEE, Bangkok, Thailand, pp. 774–779, 2009.

[15] M. Simi, P. Valdastri, C. Quaglia, A. Menciassi, P. Dario. Design, fabrication, and testing of a capsule with hybrid locomotion for gastrointestinal tract exploration. *IEEE/ASME Transactions on Mechatronics*, vol. 15, no. 2, pp. 170–180, 2010.

[16] M. Suzuki, S. Kitai, S. Hirose. Basic systematic experiments and new type child unit of anchor climber: Swarm type wall climbing robot system. In *Proceedings of IEEE International Conference on Robotics and Automation*, IEEE, Pasadena, USA, pp. 3034–3039, 2008.

[17] P. Glass, E. Cheung, M. Sitti. A legged anchoring mechanism for capsule endoscopes using micropatterned adhesives. *IEEE Transactions on Biomedical Engineering*, vol. 55, no. 12, pp. 2759–2767, 2008.

[18] P. Glass, E. Cheung, H. Wang, R. Appasamy, M. Sitti. A motorized anchoring mechanism for a tethered capsule robot using fibrillar adhesives for interventions in the esophagus. In *Proceedings of the 2nd IEEE RAS & EMBS International Conference on Biomedical Robotics and Biomechatronics*, IEEE, pp. 758–764, 2008.

[19] M. Quirini, S. Scapellato, P. Valdastri, A. Menciassi, P. Dario. An approach to capsular endoscopy with active motion. In *Proceedings of the 29th Annual International Conference of IEEE Engineering in Medicine and Biology Society*, IEEE, Lyon, France, pp. 2827–2830, 2007.

[20] A. Menciassi, P. Valdastri, C. Quaglia, E. Buselli, P. Dario. Wireless steering mechanism with magnetic actuation for an endoscopic capsule. In *Proceedings of Annual International Conference of IEEE Engineering in Medicine and Biology Society*, IEEE, Minneapolis, USA, pp. 1204–1207, 2009.

[21] F. Carpi, C. Pappone. Magnetic maneuvering of endoscopic capsules by means of a robotic navigation system. *IEEE Transactions on Biomedical Engineering*, vol. 56, no. 5, pp. 1482–1490, 2009.

[22] M. Nokata, S. Kitamura, T. Nakagi, T. Inubushi, S. Morikawa. Capsule type medical robot with magnetic drive in abdominal cavity. In *Proceedings of the 2nd IEEE RAS & EMBS International Conference on Biomedical Robotics and Biomechatronics*, IEEE, pp. 348–353, 2009.

[23] H. Yu, Y. Liu, T. Yang. Closed-loop tracking control of a pendulum-driven cart-pole underactuated system. *Journal of Systems and Control Engineering*, vol. 222, no. 2, pp. 109–125, 2008.

[24] Y. Liu, H. Yu, T. Yang. Analysis and control of a capsubot. In *Proceedings of the 17th IFAC World Congress*, IFAC, Korea, vol. 17, pp. 756–761, 2008.

[25] M. N. Huda. Analysis and Control of Propulsion Systems to be Integrated with Wireless Capsule Endoscopy, Master dissertation, Faculty of Computing, Engineering and Technology, Staffordshire University, UK, 2010.

[26] FAULHABER, [Online], Available: http://www.faulhaber-group.com/, June 6, 2011.

[27] Ansmann Racing, [Online], Available: http://www.ansmannracing.com/, June 6, 2011.

[28] H. Olsson, K. Astrom, C. Canudas de Wit, M. Gafvert, P. Lischinsky. Friction models and friction compensation. *European Journal of Control*, vol. 4, no. 3, pp. 176–195, 1998.

M. Nazmul Huda received the B. Sc. degree in electrical and electronic engineering from Bangladesh University of Engineering and Technology, Bangladesh in 2008 and MRes in robotics and control systems from Staffordshire University, UK in 2011. He is currently a Ph. D. candidate in robotics and control systems at Staffordshire University. He worked as a lecturer in the Department of Electrical and Electronic Engineering at Ahsanullah University of Science and Technology (AUST) in Bangladesh.

His research interests include robotics for medical applications, nanorobotics, and biomedical signal processing.

E-mail: m.n.huda@staffs.ac.uk (Corresponding author)

Hong-Nian Yu is currently a professor of computer science at Staffordshire University, UK. He has held several research grants worth about three million pounds from EPSRC, the Royal Society, and the EU, AWM, as well as from the industry. He has successfully completed an EU funded Asia-Link project (Euro-Asia Collaborations and Networking in Information Engineering System Technology) and currently is supervising two EU projects (East-west Link for Innovation, Networking and Knowledge exchange, 5.5 million Euro) and (Sustainable E-Tourism, 2.5 million Euro). He was the general chair of *International Conference on Software Knowledge Information Management and Applications (SKIMA)* in 2006, and is serving on various other conferences and academic societies.

His researches interests include wireless networked control systems, radio frequency identification (RFID) and its applications, mobile computing, modelling, scheduling, planning, and simulations of large discrete event dynamic systems with applications to manufacturing systems, supply chains, transportation networks, and computer networks.

E-mail: h.yu@staffs.ac.uk

Samuel Oliver Wane received the master degree in electronic engineering from the University of Hull, UK in 1996. He went on to develop software for the "Handy-1", a rehabilitation robot to aid people with no arms to feed themselves. His improvements to the robot allowed it to shave, wash, brush teeth, and play games. He then spent two years designing and developing biscuit packing robots for the food industry. Since 2000, he has been working as a senior lecturer in robotics and control at Staffordshire University, UK and a part-time Ph. D. candidate where he is developing a wirelessly controlled robot propulsion mechanism as part of the Mobile Computing and Distributed Systems (MCDS) Team.

E-mail: s.o.wane@staffs.ac.uk